HAL
open science

Optical torque reversal and spin-orbit rotational Doppler shift experiments.

Davit Hakobyan, Etienne Brasselet

To cite this version:

Davit Hakobyan, Etienne Brasselet. Optical torque reversal and spin-orbit rotational Doppler shift experiments.. Optics Express, 2015, 23 (24), pp.31230-9. 10.1364/OE.23.031230 . hal-01256744

HAL Id: hal-01256744

https://hal.science/hal-01256744v1

Submitted on 19 Jan 2016

HAL is a multi-disciplinary open access archive for the deposit and dissemination of scientific research documents, whether they are published or not. The documents may come from teaching and research institutions in France or abroad, or from public or private research centers.

L'archive ouverte pluridisciplinaire **HAL**, est destinée au dépôt et à la diffusion de documents scientifiques de niveau recherche, publiés ou non, émanant des établissements d'enseignement et de recherche français ou étrangers, des laboratoires publics ou privés.

Distributed under a Creative Commons Attribution - ShareAlike 4.0 International License

Optical torque reversal and spin-orbit rotational Doppler shift experiments

Davit Hakobyan and Etienne Brasselet*

Univ. Bordeaux, CNRS, Laboratoire Ondes et Matière d'Aquitaine, UMR 5798, F-33400 Talence, France

*etienne.brasselet@u-bordeaux.fr

Abstract: We report on optical rotational Doppler frequency shift experiments in the context of a counter-intuitive optomechanical phenomenon that is the angular analog of so-called negative optical radiation forces, which involves spin-orbit scattering of light. In practice, spin-orbit opto-mechanical effects arising from the interaction between polarized light and azimuthally varying birefringent optical elements are retrieved from mechano-optical experiments that involve spatial of the medium. Two kinds of experiments (single-beam and two-beam geometries) are performed and both approaches are discussed in the framework of previous dynamical geometric phase and rotational Doppler shift experiments based on spin and/or orbital angular momentum of light.

OCIS codes: (120.4880) Optomechanics; (050.4865) Optical vortices; (050.2555) Form birefringence; (310.6628) Subwavelength structures, nanostructures.

References and links

1. R. A. Beth, "Mechanical detection and measurement of the angular momentum of light," Phys. Rev. **50**, 115–125 (1936).
2. M. E. J. Friese, T. A. Nieminen, N. R. Heckenberg, and H. Rubinsztein-Dunlop, "Optical torque controlled by elliptical polarization," Opt. Lett. **23**, 1–3 (1998).
3. M. E. J. Friese, T. A. Nieminen, N. R. Heckenberg, and H. Rubinsztein-Dunlop, "Optical alignment and spinning of laser-trapped microscopic particles," Nature **394**, 348–350 (1998).
4. S. H. Simpson and S. Hanna, "Optical trapping of spheroidal particles in gaussian beams," J. Opt. Soc. Am. A **24**, 430–443 (2007).
5. J. Chen, J. Ng, K. Ding, K. H. Fung, Z. Lin, and C. T. Chan, "Negative optical torque," Sci. Rep. **42**, 6386 (2014).
6. D. Hakobyan and E. Brasselet, "Left-handed optical radiation torque," Nature Photon. **8**, 610–614 (2014).
7. A. Dogariu, S. Sukhov, and J. J. Saenz, "Optically induced 'negative forces,"' Nature Photon. **7**, 24–27 (2013).
8. O. Brzobohaty, V. Karasek, M. Siler, L. Chvatal, T. Cizmar, and P. Zemanek, "Experimental demonstration of optical transport, sorting and self-arrangement using a 'tractor beam,"' Nature Photon. **7**, 123–127 (2013).
9. V. Kajorndejnukul, W. Ding, S. Sukhov, C.-W. Qiu, and A. Dogariu, "Linear momentum increase and negative optical forces at dielectric interface," Nature Photon. **7**, 787–790 (2013).
10. O. V. Angelsky, A. Y. Bekshaev, P. P. Maksimyak, A. P. Maksimyak, S. G. Hanson, and C. Y. Zenkova, "Orbital rotation without orbital angular momentum: mechanical action of the spin part of the internal energy flow in light beams," Opt. Express **20**, 3563–3571 (2012).
11. K. Y. Bliokh, A. Y. Bekshaev, and F. Nori, "Extraordinary momentum and spin in evanescent waves," Nature Commun. **5**, 3300 (2014).
12. S. B. Wang and C. T. Chan, "Lateral optical force on chiral particles near a surface," Nat. Commun. **5**, 3307 (2014).
13. A. Canaguier-Durand and C. Genet, "Transverse spinning of a sphere in a plasmonic field," Phys. Rev. A **89**, 033841 (2014).
14. A. Y. Bekshaev, K. Y. Bliokh, and F. Nori, "Transverse Spin and Momentum in Two-Wave Interference," Phys. Rev. X **5**, 011039 (2015).
15. K. Y. Bliokh and F. Nori, "Transverse and longitudinal angular momenta of light," Phys. Rep. **592**, 1–38 (2015).

16. L. Marrucci, C. Manzo, and D. Paparo, "Optical spin-to-orbital angular momentum conversion in inhomogeneous anisotropic media," Phys. Rev. Lett. **96**, 163905 (2006).
17. Y. Shimotsuma, P. G. Kazansky, J. Qiu, and K. Hirao, "Self-organized nanogratings in glass irradiated by ultra-short light pulses," Phys. Rev. Lett. **91**, 247405 (2003).
18. M. Beresna, M. Gecevičius, P. G. Kazansky, and T. Gertus, "Radially polarized optical vortex converter created by femtosecond laser nanostructuring of glass," Appl. Phys. Lett. **98**, 201101 (2011).
19. G. Biener, A. Niv, V. Kleiner, and E. Hasman, "Formation of helical beams by use of Pancharatnam-Berry phase optical elements," Opt. Lett. **27**, 1875-1877 (2002).
20. M. Born and E. Wolf, *Principles of Optics* (Pergamon, 2005).
21. C. Maurer, A. Jesacher, S. Fürhapter, S. Bernet, and M. Ritsch-Marte, "Tailoring of arbitrary optical vector beams," New. J. Phys. **9**, 78 (2007).
22. G. E. Somargren, "Up/down frequency shifter for optical heterodyne interferometry," J. Opt. Soc. Am. **65**, 960–961 (1975).
23. B. A. Garetz and S. Arnold, "Variable frequency shifting of circularly polarized laser radiation via rotating half-wave retardation plate," Opt. Commun. **31**, 1–3 (1979).
24. R. Simon, H. J. kimble, and E. C. G. Sudarshan, "Evolving geometric phase and its dynamical manifestation as a frequency shift: an optical experiment," Phys. Rev. Lett. **61**, 19–22 (1988).
25. F. Bretenaker and A. L. Floch, "Energy exchange between a rotating retardation plate and a laser beam," Phys. Rev. Lett. **65**, 2316 ((1990)).
26. K. Y. Bliokh, Y. Gorodetski, V. Kleiner, and E. Hasman, "Coriolis effect in optics: unified geometric phase and spin-hall effect" Phys. Rev. Lett. **101**, 030404 (2008).
27. N. Dahan, Y. Gorodetski, K. Frischwasser, V. Kleiner, and E. Hasman, "Geometric doppler effect: spin-split dispersion of thermal radiation," Phys. Rev. Lett. **105**, 136402 (2010).
28. P. J. Allen, "A radiation torque experiment," Am. J. Phys. **34**, 1185–1192 (1966).
29. J. Courtial, K. Dholakia, D. A. Robertson, L. Allen, and M. J. Padgett, "Measurement of the rotational frequency shift imparted to a rotating light beam possessing orbital angular momentum," Phys. Rev. Lett. **80**, 3217–3219 (1998).
30. L. Allen, M. Babiker, and W. L. Power, "Azimuthal doppler shift in light beams with orbital angular momentum," Opt. Commun. **112**, 141–144 (1994).
31. G. Nienhuis, "Doppler effect induced by rotating lenses," Opt. Commun. **132**, 8–14 (1996).
32. I. Bialynicki-Birula and Z. Bialynicka-Birula, "Rotational frequency shift," Phys. Rev. Lett. **78**, 2539–2542 (1997).
33. G. Milione, S. Evans, D. A. Nolan, and R. R. Alfano "Higher order Pancharatnam-Berry phase and the angular momentum of light," Phys. Rev. Lett. **108**, 190401 (2012).
34. J. Courtial, D. A. Robertson, K. Dholakia, L. Allen, and M. J. Padgett, "Rotational frequency shift of a light beam," Phys. Rev. Lett. **81**, 3217–3219 (1998).
35. L. Chen and W. She, "Sorting photons of different rotational doppler shifts (rds) by orbital angular momentum of single-photon with spin-orbit-rds entanglement," Opt. Express **16**, 14629–14634 (2008).

1. Introduction

It is a common knowledge that light can exert torque on matter, which is associated with light-matter angular momentum exchange following the principles of mechanics. The founding experiment on optical radiation torque is that reported by Beth in 1936, who measured the spin angular momentum carried by circularly polarized light by means of a torsion pendulum made of a transparent birefringent crystal slab [1]. Several decades later, the spin angular momentum of light became a powerful tool in the development of optical manipulation techniques. Indeed, the angular degree of freedom of microparticles can be all-optically controlled via dissipative [2] or non-dissipative [3] transfer of spin angular momentum to matter, the direction of the optical torque being that of the incident spin angular momentum.

Intriguingly, a few years ago, it has been predicted that a tightly focused circularly polarized Gaussian beam could exert a torque directed oppositely to that of the incident angular momentum on wavelength-sized prolate particles made of transparent isotropic media [4]. Much more recently, the case of arrays of dielectric microspheres with wavelength size has also been investigated numerically [5] whereas the experimental identification of such counter-intuitive optical torque has been reported by using transparent space-variant form-birefringent optical elements illuminated by paraxial circularly polarized Gaussian beam [6].

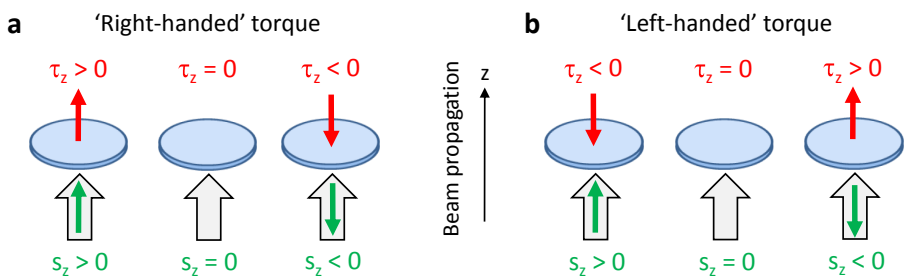

Fig. 1. Illustration of intuitive and counter-intuitive mechanical manifestations of an optical torque per photon τ_z exerted on matter by an incident Gaussian beam carrying (spin) optical angular momentum s_z per photon along its propagation direction z. (a) Right-handed situation, $s_z\tau_z > 0$ whatever s_z. (b) Left-handed situation, $s_z\tau_z < 0$ whatever s_z.

Noticeably, the angular analog of negative optical forces [6] has been introduced as a 'left-handed' effect rather than a 'negative' one, hence avoiding potential confusion with the sign of the incident angular momentum, which can be positive or negative, irrespective of whether it induces usual or counter-intuitive mechanical effects. Also, this echoes the fact that physicists usually refer to a phenomenon as being left-handed to emphasize its counter-intuitive nature. The concept is summarized in Fig. 1 where both right-handed and left-handed manifestations of the optical torque per photon τ_z, are illustrated in the case of an incident Gaussian beam propagating along the z axis and carrying a (spin) angular momentum per photon s_z. Namely the former case corresponds to $s_z\tau_z > 0$ whereas the latter situation refers to $s_z\tau_z < 0$, whatever is the value of s_z.

In fact, unconventional manifestations of mechanical effects of light attracted some attention during the past few years. In particular, several studies have been devoted to the concept of so-called negative optical forces, namely optical forces that push objects upstream of an incident photon flux, see review paper [7], whose first experimental demonstrations have been reported quite recently [8, 9]. Other examples of non-trivial optomechanics have also been observed, such as optical forces driven by the spin momentum density [10], and predicted, such as transverse optical forces and torques [11–14] that are directed perpendicular to the incident photon flux. Regarding the angular momentum of light, it is likely that its transverse and longitudinal components of both spin and orbital nature [15] will bring other optomechanical surprises in the future.

Here we present complementary experimental analysis with respect to the original report on optical torque reversal that takes place in the case of space-variant optically anisotropic transparent media [6]. Indeed, in the latter work, the observations consisted in the detection of rotational Doppler frequency shifts when such spin-orbit optical couplers are rotated around the propagation axis of the incident beam, which is associated to optical torque exerted on the sample. This was done by observing interference pattern obtained from the coherent superposition of the output beam and a non-collinear reference beam. In present study, we report on the two-beam (output and reference fields) collinear variant and single-beam (output field alone) option. Both approaches are compared and discussed in the framework of previous dynamical geometric phase and rotational Doppler shift experiments based on spin and/or orbital angular momentum of light.

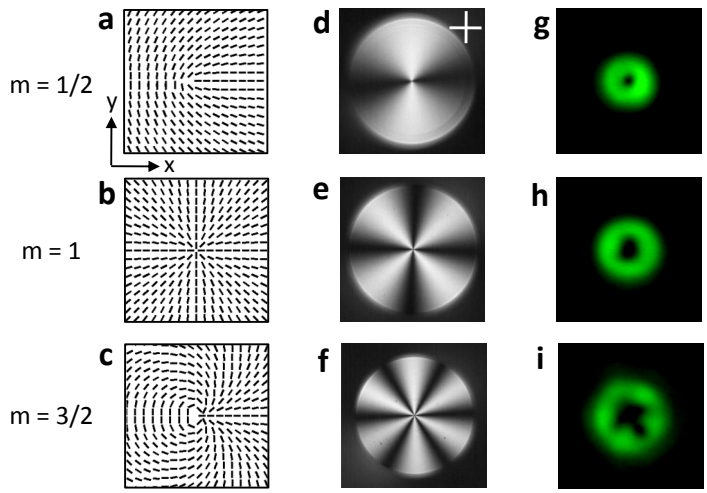

Fig. 2. Design and characterization of azimuthally varying half-wave plate retarders of azimuthal order $m = 1/2$ (upper row), 1 (middle row) and $3/2$ (bottom row) used in this work, with 532 nm operating wavelength. For each m: the left panel shows slow-axis spatial distribution in the (x,y) plane, where segments refer to the local slow-axis local orientation; the middle panel is the image of the inhomogeneous retarder observed between crossed linear polarizers whose direction are indicated as white cross in panel (d); the right panel displays output intensity profile for circularly polarized incident Gaussian beam, which corresponds to an optical vortex beam of topological charge $\pm 2m$ where the sign depends on the incident polarization state handedness.

2. Spin-orbit optomechanics of space variant birefringent media

2.1. Materials: dielectric q-plates

Following previous work [6], optical torque reversal experiments reported here are performed using nanostructured glass slabs having a uniform birefringent phase retardation of π (i.e. half-wave plate condition) for the considered wavelength (here 532 nm) and azimuthally varying optical axis orientation angle ψ of the form $\psi = m\phi$ with m half-integer and ϕ the usual polar angle in the (x,y) plane, as illustrated in Figs. 2(a)–2(c).

These anisotropic inhomogeneous optical elements, often called 'q-plates' in reference to the work by Marrucci et al. [16], have been fabricated by Altechna R&D using femtosecond laser writing of self-assembled nanostructures in silica glass. Indeed, subwavelength structuring induces form birefringence with in-plane slow/fast axis oriented perpendicular/parallel to the nanograting wavevector [17]. This is assessed experimentally by observing the samples in between crossed linear polarizers, as shown in Figs. 2(d)–2(f).

2.2. Optical consequences of spin-orbit interaction

As detailed in [18], the magnitude of the induced effective optical anisotropy can be precisely controlled by adjusting the various writing parameters. By specifying the half-wave plate condition, an incident circularly polarized paraxial Gaussian beam carrying (spin) angular momentum per photon $\sigma\hbar$ ($\sigma = \pm 1$) along the propagation axis z will emerge from the sample with a total angular momentum that is the sum of a $-\sigma\hbar$ spin contribution and a $2\sigma m\hbar$ orbital contribution [16], which accounts for a complex representation for the electric field of the form $\exp(-i\omega t + ikz)$ with ω the angular frequency of light, k the wavevector and time t.

In other words, an incident circularly polarized paraxial Gaussian beam is transformed into a contra-circularly polarized optical vortex beam carrying on-axis optical phase singularity with topological charge $2\sigma m$. In fact, this can be easily grasped by evaluating the Jones matrix of a static q-plate of order m in the circular polarization basis $(\mathbf{c}_+, \mathbf{c}_-)$, with $\mathbf{c}_\sigma = (\mathbf{x} + i\sigma\mathbf{y})/\sqrt{2}$. Namely, up to an unimportant phase factor,

$$\mathbf{J}^{(m)}_{\text{static}} = \begin{pmatrix} 0 & e^{+2im\phi} \\ e^{-2im\phi} & 0 \end{pmatrix}. \tag{1}$$

Optical vortex generation is therefore described by applying $\mathbf{J}^{(m)}_{\text{static}}$ on the incident Jones vector $(1,0)^T$ when $\sigma = 1$ or $(0,1)^T$ when $\sigma = -1$, X^T being the transpose of X.

This is experimentally illustrated in Figs. 2(g)–2(i) where the output doughnut-shaped intensity pattern is shown for $m = 1/2$, 1 and $3/2$. Such optical spin-orbit interaction phenomenon that couples the spin and orbital angular momentum contributions of light finds its origin in the geometric phase arising from the spatial rotation of the local coordinate frame attached to the anisotropy axis [19].

2.3. Mechanical consequences of spin-orbit interaction

Besides optical vortex generation from spin-orbit interaction, mechanical effects may also occur. Indeed, angular momentum conservation of the light-matter system implies that an optical radiation torque τ_z per photon is exerted on the spin-orbit coupler. More precisely, under incident circularly polarized Gaussian beam with helicity σ, one has

$$\tau_z^{(\sigma)} = \tau^{(\sigma)}_{z,\,\text{spin}} + \tau^{(\sigma)}_{z,\,\text{orbital}}, \tag{2}$$

where the spin and orbital contribution to the total torque are respectively $\tau^{(\sigma)}_{z,\,\text{spin}} = 2\sigma\hbar$ and $\tau^{(\sigma)}_{z,\,\text{orbital}} = -2\sigma m\hbar$, which gives

$$\tau_z^{(\sigma)} = 2\sigma(1-m)\hbar. \tag{3}$$

More generally, in the case of an elliptically polarized incident beam characterized by the ellipticity angle χ [20] ($-\pi/4 \leq \chi \leq \pi/4$), which carries $\hbar\sin 2\chi$ spin angular momentum per photon, the optical radiation torque can be found by decomposing the incident field on the circular polarization basis. One obtains

$$\tau_z^{(\chi)} = \frac{1}{2}\left[(1+\sin 2\chi)\,\tau_z^{(+)} + (1-\sin 2\chi)\,\tau_z^{(-)}\right], \tag{4}$$

hence

$$\tau_z^{(\chi)} = 2\sin 2\chi\,(1-m)\hbar. \tag{5}$$

Right-handed optical torque, $\tau_z^{(\chi)}\sin 2\chi > 0$, is thus obtained for $m < 1$ whereas left-handed situation, $\tau_z^{(\chi)}\sin 2\chi < 0$, occurs for $m > 1$ when the radiation torque is dominated by the orbital contribution rather than that of the spin. On the other hand, the particular case $m = 1$ gives zero torque, which is a mere consequence of the rotational invariance of the medium around the z axis. The case of an incident linearly polarized Gaussian beam ($\chi = 0$) also leads to zero net torque but this results from the exact compensation between the respective contributions of the two circular components of the field.

2.4. *Experimental approach*

Optical radiation torque reversal is here addressed by considering two distinct rotational Doppler shift experiments performed using a continuous-wave laser source operating at 532 nm wavelength. Both experiments, which consist to rotate the sample around the z axis at constant angular frequency Ω, are presented and analyzed in the next section.

The main idea is to probe the opto-mechanical effect of light on the q-plate from the assessment of the mechano-optical effect of the rotating q-plate on light, thereby circumventing the practical difficulty associated with the direct observation of light-induced rotation. Indeed, as previously discussed in [6], the fact that a circularly polarized incident beam exerts a nonzero optical radiation torque (which implies $m \neq 1$) on the sample is associated with a rotational Doppler frequency shift $\delta\omega$ imparted to the output contra-circularly polarized light field as the q-plate is rotated. The expression of the frequency shift can be derived following energy conservation principle for the 'light+matter' system considered as isolated, namely $w + \hbar\delta\omega = 0$ where $w = \tau_z\Omega$ is the work per photon produced on the slab, which gives

$$\delta\omega = 2\sigma\Omega(m-1)\,. \tag{6}$$

It is also instructive to retrieve Eq. (6) from Jones formalism by evaluating the time-dependent Jones matrix that describes the rotating q-plate. First, we note that the optical axis orientation angle ψ, in the fixed reference frame (x,y,z), is rotated by an angle $(1-m)\varphi$ when the sample is rotated by an angle φ around the z axis. The dynamical Jones matrix in the circular polarization basis is thus obtained from Eq. (1) by applying the transformation $\psi \to \psi + (1-m)\Omega t$, assuming that the static q-plate starts to rotate with angular velocity Ω at $t = 0$. This gives

$$\mathbf{J}^{(m)}_{\text{dynamic}} = \begin{pmatrix} 0 & e^{+2i[m\phi+(1-m)\Omega t]} \\ e^{-2i[m\phi+(1-m)\Omega t]} & 0 \end{pmatrix}. \tag{7}$$

According to the adopted complex representation mentioned above that implies angular frequency definition of the form $-\partial\Phi/\partial t$, where Φ denotes the phase of the optical field, one thus retrieves from Eq. (7) the expression for the frequency shift given by Eq. (6).

3. Spin-orbit rotational Doppler shift experiments

3.1. *Two-beam experiment*

In a first set of experiments we have accessed to rotational Doppler shift by using the setup shown in Fig. 3. In practice, the temporal behavior of interferograms obtained using a Mach-Zehnder interferometer is video recorded. Such interferogram consists of the collinear coherent superposition of the output light field with a reference Gaussian beam whose circular polarization state is orthogonal to that of the incident Gaussian beam. The q-plate is rotated at constant angular velocity $\Omega \approx 0.4$ rad/s by placing the samples on a motor-controlled rotating stage. The results are shown in Fig. 4 for $m = (1/2, 1, 3/2)$.

For each m, a snapshot of the $2|m|$-arm spiraling intensity pattern observed in the (x,y) plane is shown in Figs. 4(a)–(c). The dynamics of the latter pattern is quantitatively retrieved by looking at the time dependence of the correlation coefficient C between the intensity patterns at time 0 and t, see Figs. 4(d)–(f) that correspond to 120 seconds acquisition time duration. The observed time dependence of $C(t)$ as a function of m follows the predicted dependence of the frequency shift $\delta\omega$ given by Eq. (6). Indeed, overall static behavior is found for $m = 1$, which is basically associated with the rotational invariance around the z axis of the q-plate. In contrast, when $m \neq 1$, $C(t)$ exhibits sinusoidal behavior with angular frequency Ω_C that satisfies the expected relationship $\Omega_C = |\delta\omega| = 2|(m-1)\Omega|$. Indeed, data fitting gives $\Omega_C = 0.36$ rad/s for $m = 1/2$ and $\Omega_C = 0.40$ rad/s for $m = 3/2$.

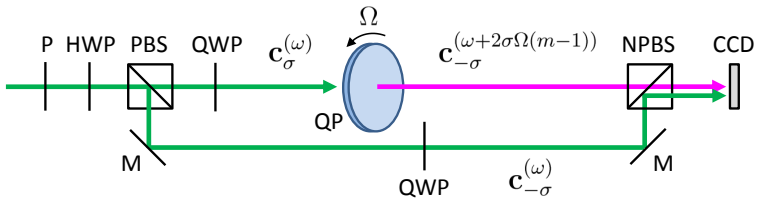

Fig. 3. Sketch of the two-beam rotational Doppler experimental set-up used to videorecord the interference pattern between (i) the frequency shifted output beam emerging from the sample, labeled $\mathbf{c}_{-\sigma}^{(\omega+2\sigma\Omega(m-1))}$, illuminated by collimated circularly polarized Gaussian beam with waist radius $w \approx 1$ mm and helicity σ, $\mathbf{c}_{\sigma}^{(\omega)}$, and (ii) a collinear reference beam with helicity $-\sigma$, $\mathbf{c}_{-\sigma}^{(\omega)}$. Optical elements: P is linear polarizer, HWP is half-wave plate, QWP is quarter-wave plate, QP is q-plate, M is mirror, PBS is polarizing beam splitter, NPBS is non-polarizing beam splitter, CCD is imaging device.

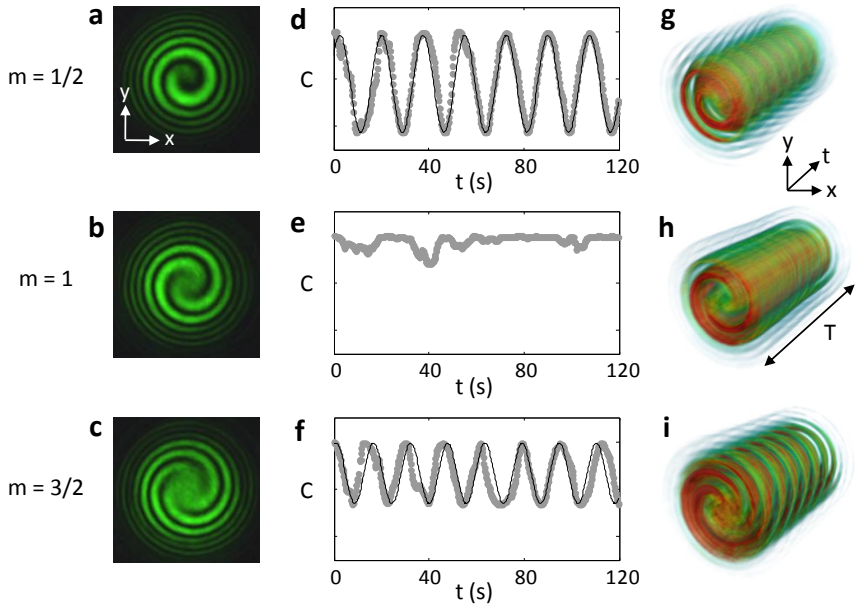

Fig. 4. Two-beam rotational Doppler experimental results for $m = 1/2$ (upper row), $m = 1$ (middle row) and $m = 3/2$ (bottom row) by using the set-up depicted in Fig. 3. For each m: left panel displays a snapshot of the interference intensity pattern observed in the (x, y) plane at $t = 0$; middle panel shows the time dependence of the correlation coefficient C between intensity patterns at $t = 0$ and t where the solid line (for $m = 1/2$ and $3/2$) refers to fit by sinusoidal function, see text for details; right panel is a volumetric representation of the recorded interferogram in the (x, y, t) spatiotemporal frame during $T = 120$ s.

Remarkably, the reminiscence of optical torque reversal from a right-handed to a left-handed situation while the input angular momentum is kept fixed as m increases from $1/2$ to $3/2$ [see the factor $m - 1$ in Eq. (5)] is retrieved from the space-time representation of the interferograms shown in Figs. 4(g)–(i). Indeed, handedness reversal of the screw-shaped spatiotemporal interferograms is observed when passing from $m = 1/2$ [Fig. 4(g)] to $m = 3/2$ [Fig. 4(i)].

3.2. *Single-beam experiment*

Following the sketch shown in Fig. 5, reference-free interference pattern can also be obtained by using a linearly polarized (here along the x axis) incident Gaussian beam instead of a circularly polarized one. Indeed, the incident field can be described in that case as a coherent superposition of orthogonally polarized circularly polarized identical Gaussian beams, each of them exerting on the sample an optical radiation torque with equal magnitude and opposite sign. Although the total torque exerted on the sample is zero, the individual optomechanical contributions of each circularly polarized component of the incident field can nevertheless be retrieved by rotating the sample at constant angular frequency Ω.

Practically, this is done by projecting the output field along the y axis by placing a linear polarizer after the sample, as depicted in Fig. 5. This allows orthogonal circularly polarized output components to interfere and produce a $4|m|$-fold rotationally symmetric patterns in the (x,y) plane, as illustrated in the insets of Fig. 6 that correspond to the situation at rest. More precisely, the output field just after the q-plate is described by

$$\mathbf{E}^{(m,\Omega=0)}_{\text{after QP}} = \mathbf{J}^{(m)}_{\text{static}}\,(1/\sqrt{2},1/\sqrt{2})^T = \cos(2m\phi)\,\mathbf{x} + \sin(2m\phi)\,\mathbf{y}\,. \tag{8}$$

The corresponding beam is characterized by an azimuthally varying linear polarization state that results from the superposition of two contra-circularly polarized vortex beams of opposite topological charges $\pm 2m$ and is known as a vector beam, see for instance [21]. From Eq. (8), the projection on the output linear polarizer thus gives a beam with azimuthally modulated intensity proportional to $\sin^2(2m\phi)$. When the sample is rotated around the z axis, the azimuthally modulated intensity pattern acquires a dynamical behavior for $m \neq 1$, as shown in Figs. 6(a)–6(c) that present the volumetric rendering of the spatiotemporal intensity pattern for $m = (1/2, 1, 3/2)$ over two full rotations of the sample; here the angular velocity is $\Omega = 0.44$ rad/s with corresponding time duration $T \approx 30$ s. Such a behavior is reminiscent of oppositely frequency shifted circular components that emerge from non-axisymmetric samples. The underlying optical torque reversal for the situations $m = 1/2$ and $m = 3/2$ is grasped from spatiotemporal patterns with opposite handedness. In fact these observations can be retrieved by evaluating the projection on the output polarizer of the dynamical Jones vector that emerges from the rotating q-plate,

$$\begin{aligned} \mathbf{E}^{(m,\Omega)}_{\text{after QP}} &= \mathbf{J}^{(m)}_{\text{dynamic}}\,(1/\sqrt{2},1/\sqrt{2})^T\,, \\ &= \cos(2[m\phi + (1-m)\Omega t)]\,\mathbf{x} + \sin(2[m\phi + (1-m)\Omega t)]\,\mathbf{y}\,, \end{aligned} \tag{9}$$

which gives

$$\mathbf{E}^{(m,\Omega)}_{\text{after P}_{\text{out}}} = \sin(2[m\phi + (1-m)\Omega t)]\,\mathbf{y}\,. \tag{10}$$

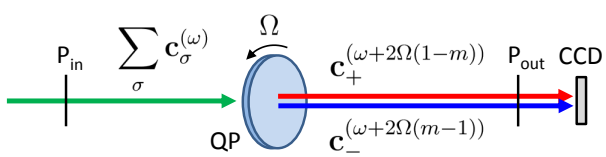

Fig. 5. Single-beam rotational Doppler experimental sketch that aims at videorecording the interference pattern between the two frequency shifted circular components $\mathbf{c}_\sigma^{(\omega+2\sigma\Omega(1-m))}$, owing to the output polarizer oriented along the y axis for linearly polarized incident Gaussian beam along the x axis with waist radius $w \approx 1$ mm. Optical elements: $P_{\text{in/out}}$ are input/output linear polarizers, QP is q-plate, and CCD is imaging device.

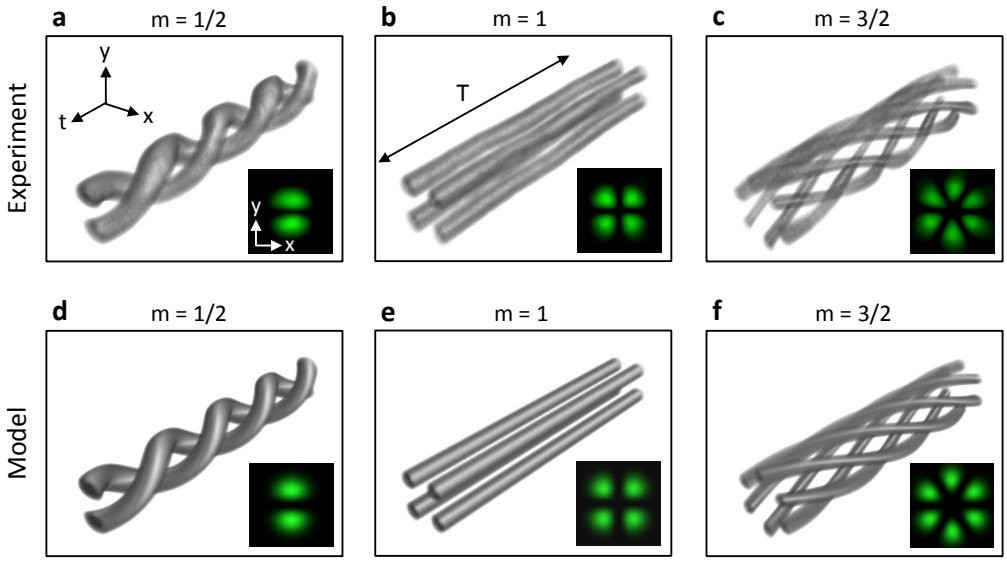

Fig. 6. Single-beam rotational Doppler experiment for $m = 1/2$ (left column), $m = 1$ (middle column) and $m = 3/2$ (right column) following the set-up shown in Fig. 5. Snapshot of the intensity profile in the (x, y) plane of the linearly polarized output component that is orthogonal to that of a linearly polarized incident Gaussian beam is shown in the inset of each panel whereas the spatiotemporal behavior are represented with volumetric rendering over a duration that corresponds to two full rotations of the sample, $T \approx 30$ s. Upper row: experiment. Bottom row: model.

The resulting intensity pattern thus has angular frequency $[(m-1)/m]\Omega$, which matches with the observed time-periodic behavior in Figs. 6(a)–6(c). Assuming a radial dependence of the output beam of the form of a paraxial Laguerre-Gaussian beam with azimuthal index $l = 2m$ and radial index $p = 0$ (which formally neglects the radial modal content of the field generated by the q-plate, but does not affect qualitatively the predictions) the corresponding spatiotemporal intensity pattern is described as

$$I(r,t) = (r/w)^{4|m|} \exp(-2r^2/w^2) \sin^2(2[m\phi + (1-m)\Omega t]), \tag{11}$$

where w is the beam waist radius, see Figs. 6(d)–6(f) and a fair agreement with experimental data is obtained.

4. Discussion and conclusion

Early rotational Doppler frequency shift experiments were performed with uniform uniaxial optical retarders, namely rotating half-wave plates [22, 23] where the frequency shift imparted to light has been treated using Jones formalism. Later, variants have been also reported, for instance using a rotating quarter-wave plate, albeit described from the point of view of the geometric phase [24]. Still, in [24], Simon et al. have emphasized the equivalence of the rotational Doppler effect and geometric phase in systems with rotating elements. Such an equivalence has been rediscussed later in the framework of energy conservation considerations in [25] by Bretenaker and Le Floch, who also provided identical conclusions supported by experimental observations. Rotational Doppler shift experiments have also been extended to the case of orbital angular momentum [29], which has provided experimental foundations to earlier theoretical predictions [30–32]. On the other hand, present work should also be replaced in the context

of vector beams since they are involved in the single-beam experiment. Indeed, when rotated, a vector beam acquires a geometric phase that is related to its rotational symmetry [33]. Since in our case the generated vector beam is put into rotation, see Eq. (9), the measured rotational frequency shift manifests as a dynamical geometric phase for vector beams.

From a general point of view, the equivalence mentioned above is not restricted to propagating fields and also holds for surface waves as reported for instance by Bliokh et al. in [26] in the case of visible domain radiation ($\lambda \sim 0.5\ \mu$m) and by Dahan et al. in [27] in the case of thermal radiation ($\lambda \sim 10\ \mu$m).

Noticeably, the connection between optical radiation torque driven by the spin angular momentum of light and rotation-induced frequency shift has been discussed a long time before above mentioned works, in the case of a microwave experiment [28].

In such context, present experiments carried out with space-variant optically anisotropic structures, which are basically spin-orbit scattering transparent optical elements, constitute an optomechanical spin-orbit approach to the long-lasting topic of optical rotational Doppler frequency shifts, dynamical geometric phase and angular momentum of light. In particular we mention the unified picture in terms of the Coriolis effect reported in [26] and that is associated to observations in a noninertial reference frame, noting that in our case it is the medium that rotates instead of the observer; in turn one passes from one situation to another by mere change of sign of the involved angular velocity.

We also note that the spin-orbit version proposed here shares some analogy with previous experimental work regarding the additive contribution of the spin and orbital angular momentum components of light to the frequency shift [34]. Moreover, our results bring an an experimental playground to previous theoretical study that discussed the use of spin-orbit rotational Doppler frequency shifts for encoding an extra degree of freedom into a light field [35]. Finally, as far as optomechanics itself is concerned, we stress that the direct experimental observation of a left-handed optical radiation torque is still an open issue at present day on which we should hopefully report in a near future.

Acknowledgment

This study has been carried out with financial support from the French State, managed by the French National Research Agency (ANR) in the frame of “the Investments for the future” Programme IdEx Bordeaux – LAPHIA (ANR-10-IDEX-03-02).